Journal of the Optical Society of America B
OPTICAL PHYSICS

Recent advances in supercontinuum generation in specialty optical fibers [Invited]

T. Sylvestre,[1,*] E. Genier,[1,2] A. N. Ghosh,[1,3] P. Bowen,[4] G. Genty,[5] J. Troles,[6] A. Mussot,[2] A. C. Peacock,[3] M. Klimczak,[7] A. M. Heidt,[8] J. C. Travers,[9] O. Bang,[4,10] and J. M. Dudley[1]

[1]Institut FEMTO-ST, UMR 6174 CNRS-Université Bourgogne Franche-Comté, 25030 Besançon, France
[2]Université de Lille, CNRS, UMR 8523-PhLAM-Physique des Lasers Atomes et Molécules, F-59000 Lille, France
[3]Optoelectronics Research Centre, University of Southampton, Southampton, SO17 1BJ, UK
[4]NKT Photonics A/S, Blokken 84, DK-3460, Birkerød, Denmark
[5]Photonics Laboratory, Tampere University, FI-33104 Tampere, Finland
[6]Université de Rennes, CNRS, ISCR-UMR 6226, 35000 Rennes, France
[7]Faculty of Physics, University of Warsaw, Pasteura 5, 02-093 Warsaw, Poland
[8]Institute of Applied Physics, University of Bern, Bern, Switzerland
[9]School of Engineering and Physical Sciences, Heriot-Watt University, Edinburgh, EH14 4AS, UK
[10]DTU Fotonik, Department of Photonics Engineering, Technical University of Denmark, 2800 Kgs. Lyngby, Denmark
*Corresponding author: thibaut.sylvestre@univ-fcomte.fr

Received 3 August 2021; accepted 18 September 2021; posted 29 September 2021 (Doc. ID 439330); published 25 October 2021

The physics and applications of fiber-based supercontinuum (SC) sources have been a subject of intense interest over the last decade, with significant impact on both basic science and industry. New uses for SC sources are also constantly emerging due to their unique properties that combine high brightness, multi-octave frequency bandwidth, fiber delivery, and single-mode output. The last few years have seen significant research efforts focused on extending the wavelength coverage of SC sources towards the 2 to 20 μm molecular fingerprint mid-infrared (MIR) region and in the ultraviolet (UV) down to 100 nm, while also improving stability, noise and coherence, output power, and polarization properties. Here we review a selection of recent advances in SC generation in a range of specialty optical fibers, including fluoride, chalcogenide, telluride, and silicon-core fibers for the MIR; UV-grade silica fibers and gas-filled hollow-core fibers for the UV range; and all-normal dispersion fibers for ultralow-noise coherent SC generation.

https://doi.org/10.1364/JOSAB.439330

1. INTRODUCTION

A longstanding challenge since the invention of the laser has been the development of efficient methods to exploit nonlinearity to convert laser light to new wavelengths. Supercontinuum (SC) generation in optical fibers has been shown to offer a convenient and elegant solution to this challenge, as it massively broadens the laser spectrum while maintaining a spatially coherent output [1,2]. This provides an inherently fiber-delivered broadband light spectrum possessing the brightness of a laser and the spectral width of a lamp, capable of replacing most light sources used today in optical metrology, spectroscopy, and microscopy. Important applications of fiber-based broadband SC sources include bio-imaging, optical coherence tomography (OCT), material processing, optical sensing, absorption spectroscopy, and optical frequency comb (OFC) technologies [1–5]. Many applications also benefit from the fact that SC light is several orders of magnitude spectrally brighter than blackbody radiation, and its coherence properties enable the use of relatively simple interferometric and heterodyne detection schemes.

State-of-the-art commercial SC fiber sources are mostly based on silica-glass photonic crystal fibers (PCFs), providing watt-level output power over the complete silica fiber transmission window, i.e., from 400 to 2400 nm. Fluoride-fiber-based mid-infrared (MIR) SC sources with spectra reaching up to 4 μm (in some cases up to 4.8 μm) have also become commercially available [6,7]. However, many emerging applications require extension of the SC spectrum beyond the state of the art, towards both the (ultraviolet) UV range (ideally from 50 to 400 nm) and the MIR range from 2 to 20 μm. There is particular need for broadband sources of UV light for fluorescence imaging and for diagnostic and therapeutic uses in medicine [8], and the MIR covers the molecular fingerprint region and the atmospheric windows of 3−5 μm and 8−12 μm [9,10]. Covering this MIR range is necessary for OCT imaging, remote sensing, air pollution monitoring, homeland security, and minimally invasive medical surgery [11–19].

Recent years have seen significant progress in overcoming the current shortcomings of SC sources in terms of wavelength coverage, noise, power density, and robustness. Significant developments have been made in reaching target UV and MIR wavelength ranges, and the fiber SC has matured considerably to become a truly disruptive technology able to meet a range of societal and industrial challenges.

A key reason for these advances has been the development of new classes of specialty optical fiber, and the purpose of this paper is to present a review of this work. The paper is organized as follows. The second section introduces the physics of SC generation and presents an overview of the approaches and techniques used for fiber-based SC generation. In Section 3, we provide a brief review of recent results in MIR SC generation in soft-glass fibers using direct and cascaded pumping. We specifically describe work developing compact and reliable MIR SC sources based on fiber laser pumped cascaded fiber systems. A short segment is then devoted to the new silicon-core fibers for SC applications. While IR fiber SC technology is becoming more and more robust, SC generation in the UV is still a developing area. In Section 4, we describe the different specialty fibers for UV SC generation, including gas-filled hollow-core (HC) fibers and UV-grade silica fibers. In Section 5, we discuss recent achievements developing low-noise and coherent SC sources based on all-normal dispersion (ANDi) PCFs, as well as present an overview of potential applications.

To introduce the topics covered in this review, it is useful to begin by presenting a summary of the various SC bandwidths that have been reported using different optical fiber platforms. Figure 1 presents a survey of fiber SC spectral coverage from the UV (100 nm) to MIR ranges up to 20 μm. These include standard silica-based PCF SC source from 400 nm to 2.4 μm, UV-grade (high-OH-dopant) silica fibers (OH) for UV extension down to 300 nm [20], and highly GeO_2-doped silica fibers (Ge) for IR extension up to 3.2 μm [21]. The survey also shows the SC bandwidths achieved using heavy-metal oxide (HMO) fibers, fluoride-glass fibers up to 4.8 μm, chalcogenide-glass fibers up to 18 μm, and liquid-core and gas-filled HC fibers. The insets show scanning electron microscope (SEM) images of some of the different PCF platforms used for SC generation, including (left) ANDi PCF and suspended-core PCF, (top right) HC anti-resonant fiber (HC-ARF) and photonic bandgap (PBG)-PCF, and (bottom right) ZBLAN fiber, HMO-PCF, and chalcogenide (AS_2Se_3) PCF.

2. SUPERCONTINUUM PHYSICS

There have been many attempts to control and harness nonlinear and spectral broadening dynamics in silica fibers [22], but it was truly the advent of the microstructured air-hole fiber (PCF) in the mid 1990s that revolutionized the generation of broadband SC [23,24]. In particular, PCFs have allowed tailoring of the fiber dispersion while increasing the efficiency of nonlinear effects leading to SC spectra extending over the full transmission window of silica fibers, and enabling applications outside laboratories. A key aspect in the success of PCFs for SC generation was to match the zero-dispersion wavelength (ZDW) with the wavelength of available ultrafast laser systems, enabling efficient seeding of soliton dynamics that underpin spectral broadening [25].

Temporal solitons are remarkably robust nonlinear optical waves formed under the proper balance between linear dispersion and nonlinear self-phase modulation (SPM). Exciting soliton dynamics requires injecting short pulses in the anomalous dispersion regime of a fiber, which in most cases corresponds to pumping at wavelengths longer than the fiber ZDW. In this regime, the input pulse experiences an initial

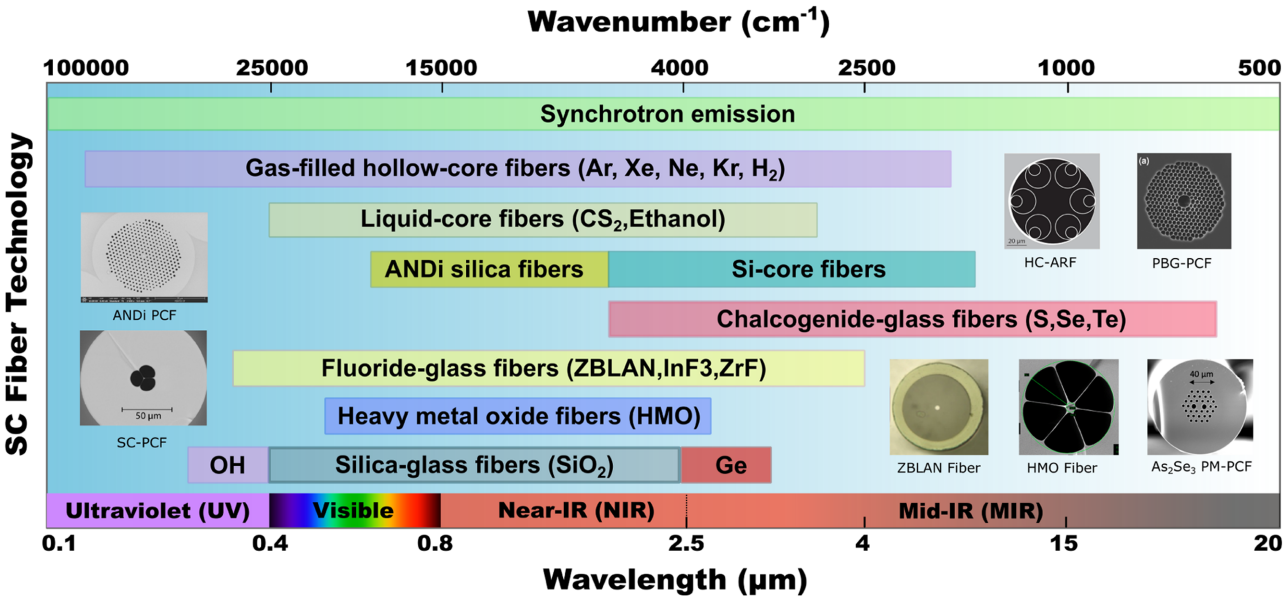

Fig. 1. Survey of SC bandwidths in various specialty optical fibers from ultraviolet (UV) to MIR ranges. The insets show some examples of the different fiber platforms used for SC generation, including (left) all-normal dispersion (ANDi) PCF and suspended-core PCF, (top right) hollow-core anti-resonant fiber (HC-ARF) and photonic bandgap (PBG-PCF), (bottom right) fluoride-glass (ZBLAN) step-index fiber, heavy-metal-oxyde (HMO-PCF), and chalcogenide (AS_2Se_3) polarization-maintaining (PM) PCF.

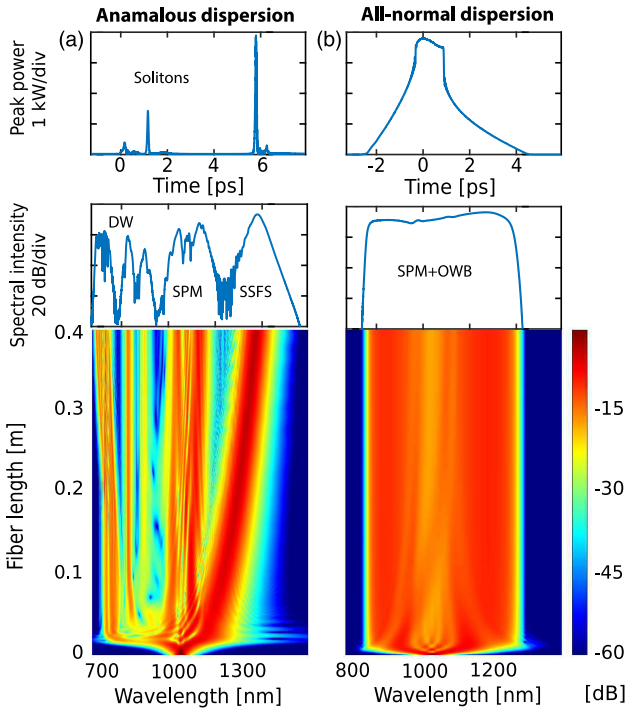

Fig. 2. Numerical simulations based on the generalized nonlinear Schrödinger equation of (a) anomalous and (b) ANDi SC generation as a function of propagation distance in the fiber. The input parameters are 50 fs pulse duration at 1040 nm with 10 kW peak power and $\beta_2 = -11$ ps^2.km^{-1} for (a) and with 50 kW peak power and $\beta_2 = 5.27$ ps^2.km^{-1} for (b).

stage of higher-order soliton compression and fission into fundamental solitons. Perturbation of the soliton dynamics by higher-order dispersion and stimulated Raman scattering (SRS) leads to the emission of dispersive waves (DWs) in the visible and soliton self-frequency shift (SSFS) towards the IR [25]. A numerical illustration of these processes is shown in Fig. 2(a), which plots the typical spectral evolution of a 50 fs input hyperbolic secant pulse at 1040 nm in the anomalous dispersion regime of a single-mode silica PCF. The simulation is based on the general nonlinear Schrödinger equation (GNLSE) solved with the split-step method [25] and using parameters as given in the figure caption. The nonlinear dynamics are primarily governed by the fiber dispersion profile, and a wide variety of dispersion-engineered PCFs have been designed and fabricated to match the ZDW with various pump lasers around 800 nm, 1040 nm, 1064 nm, 1550 nm, 2 μm, and beyond. Much effort has also been dedicated to design PCFs with two ZDWs (parabolic dispersion), enabling solitons to emit far-detuned DWs on both sides of the SC spectrum [26].

Although soliton-based SC generation is known to yield the broadest SC spectra, SC generation in ANDi fibers developing from SPM and optical wave breaking (OWB) has also been extensively studied. ANDi SC requires higher-peak-power femtosecond pulses and leads to pulse-preserved, flat-top, fully coherent SC spectra as confirmed by numerical simulations [see Fig. 2(b)] [27]. These features make ANDi SC of particular interest for applications requiring high coherence as well as uniform and smooth spectral and temporal intensity profiles. However, despite relative abundance of results on ANDi PCF and coherent SC generation demonstrations in the literature (see Section 5 for a detailed review), there is a lack of detailed experimental characterization of the spectro-temporal properties of ANDi SC pulses. A recently published study exploiting time-domain ptychography for full-field characterization [28] has revealed the importance of using high-quality pump pulses for the generation of stable SC. In particular, this study has shown that ANDi SC pulses may exhibit complex temporal fine structure on time scales of a few optical cycles arising from the nonlinear amplification of imperfections of the pump pulse such as pre-/post-pulses and low-level pedestals [29]. These results somewhat contrast the general perception that ANDi SC inherently possess continuous and uniform spectrograms as typically seen in numerical simulations assuming ideal femtosecond pump pulses [30]. However, taking into account the full-field characteristics of the pump pulses (e.g., retrieved from a frequency-resolved optical gating measurement) in GNLSE simulations enabled the reconstruction of the observed ANDi SC pulse complexity in remarkable agreement with the experimental measurements. It further enabled linking the observed temporal fine structure features to specific fiber parameters such as birefringence [29].

SC generation in silica PCFs has been observed using not only ultrashort femtosecond seed pulses but also using longer picosecond or nanosecond pulses [31–33], and even in the continuous-wave (CW) regime [34–37]. In the long pulse regime, the key nonlinear process underlying SC generation in the anomalous dispersion region is noise-seeded modulation instability (MI), which breaks up the input pulse envelope into a train of hundreds sub-picosecond breather pulses with random characteristics (amplitude and duration) that subsequently undergo soliton dynamics similar to those observed in the short pulse regime [38]. In the normal dispersion regime, the SC develops from the combined effects of noise-seeded parametric four-wave mixing (FWM) processes assisted by cascaded Raman scattering (CRS) [39–41]. In multimode or birefringent fibers, the FWM processes can originate from phase-matched intermodal and vectorial nonlinear instabilities, including polarization MI (PMI) and cross-phase MI (XPMI), respectively. Dual-pumping schemes have also been implemented for multi-octave spanning SC generation based on cross-phase modulation (XPM) [42].

More recently, SC generation has also been reported in graded-index (GRIN) multimode optical fibers, triggered by geometric parametric instability due to periodic self-imaging arising from multimodal interference, which can under particular injection conditions lead to the generation of broadband self-cleaned beam output [43–45]. SC generation in liquid-core optical fibers (LiCOFs) has also seen increased interest in recent years due to the high refractive index and wide MIR spectral transparency of inorganic solvents. A particular feature associated with liquids from the nonlinear physics viewpoint is their non-instantaneous nonlinearity and stimulated nonlinear scattering arising from the slow molecular motion of liquids, characteristics that give rise to specific nonlinear dynamics and allow for highly coherent SC generation [46–49].

3. MIR SUPERCONTINUUM GENERATION

SC generation in the MIR regime has been extensively investigated in the past 15 years with more than 400 scientific papers published on this topic. It is still a very active field of research, driven by a wide range of potential applications, including molecular spectroscopy, OCT, material processing, and optical sensing [9–19].

A. Soft-Glass Fibers

The development of MIR SC sources poses a number of important challenges due to the requirement of non-silica soft glasses, complex fabrication techniques, and new pump laser wavelengths. Significant efforts have been devoted to the synthesis of soft glasses for the MIR [50,51], including chalcogenide arsenic trisulfide (As_2S_3), arsenic triselenide (As_2Se_3), germanium arsenic selenide (GeAsSe), germanium telluride (GeTe and GeAsTeSe) [9,52,53], tellurite (TeO_2) [54,55], chalcohalides (Ge–Te–AgI) [56], HMO ($PbO-Bi_2O_3-Ga_2O_3-iO_2-CdO$) [57], and fluorides (ZBLAN : $ZrF_4-BaF_2-LaF_3-AlF_3$–NaF; InF_3; ZrF_4) [58–60]. Among the large variety of IR fibers, chalcogenide-glass-based fibers (composed of chalcogen elements such as S, Se, or Te) are excellent platforms for SC applications in the MIR due to their wider transmission window, tailorable dispersion, and hundred times larger nonlinearity compared to silica or ZBLAN fibers [9,52,61–63]. Bulk chalcogenide glasses are usually prepared using several techniques such as melt-quenching [51,64] or microwave radiation [65,66], which can be drawn into highly nonlinear step-index fibers [64] or dispersion-tailored PCFs using techniques such as molding [67–69], drilling [70], and extrusion [71].

Below, we present a brief review of the state of the art for MIR SC generation in soft-glass fibers, classified into direct pumping and cascaded pumping. Direct pumping is based on bulky and expensive MIR pump laser sources such as tunable optical parametric oscillators (OPOs) and optical parametric amplifiers (OPAs), which can suffer from low output power and poor stability. Cascaded systems based on fiber lasers and MIR nonlinear fibers have recently emerged as attractive and promising alternatives, opening routes towards practical, table-top, and robust MIR SC sources with high spectral power density. Of particular interest are compact and reliable all-fiber systems pumped with standard fiber lasers at telecommunication wavelengths where an initial pulse at a wavelength of 1550 nm is gradually shifted towards longer wavelengths in a cascade of silica and soft-glass fibers, enabling a stepwise extension to the MIR. From a fundamental physics viewpoint, the cascade allows for strongly enhancing the SSFS dynamics using dispersion-engineered and highly nonlinear fiber segments, enabling extension of the SC far into the MIR [72].

Among the direct pumping SC generation systems, Cheng *et al*. have reported the generation of a SC spanning from 2−15.1 μm in a 3 cm long step-index As_2Se_3 fiber [61]. The fiber with a core diameter of 15 μm was pumped at 9.8 μm with a peak power of 2.89 MW delivered from a MIR pump source comprising a Ti:sapphire mode-locked seed laser, a traveling-wave OPA of superfluorescence (TOPAS), and a difference frequency generation (DFG) unit [61]. Ou *et al*. also reported a MIR SC spectrum spanning from 1.8 to 14 μm in a 20 cm long and 23 μm core diameter $Ge_{15}Sb_{25}Se_{60}/Ge_{15}Sb_{20}Se_{65}$ step-index fiber pumped by 150 fs pulses at 6 μm delivered by an OPA system [73]. Using an ultrahigh numerical aperture chalcogenide step-index fiber, C.R. Petersen *et al*. demonstrated a SC spectrum covering from 1.4 to 13.3 μm, and with an output power of 150 μW with potential for upscaling by increasing the repetition rate or the pulse duration [9]. The spectral broadening was achieved by pumping a 16 μm core diameter fiber made from $As_{40}Se_{60}/Ge_{10}As_{23.4}Se_{66.6}$ (core–cladding) glass at 6.3 μm using a Ti:sapphire laser pumped tunable OPA and noncollinear DFG module. Yu *et al*. reported the widest spectrum in step-index chalcogenide fibers with a low peak power of 3 kW [74]. By pumping an 11 cm long $Ge_{12}As_{24}Se_{64}/Ge_{10}As_{24}S_{66}$ fiber with 330 fs pulses at 4.0 μm emitted from an OPA system, they obtained a SC spectrum spanning from 1.8 to 10 μm [74].

Many chalcogenide fibers contain elements such as arsenic and antimony, which can be associated with possible safety issues during glass synthesis, fiber drawing, and testing. Research has thus also been devoted to remove arsenic and antimony elements from chalcogenide glasses, while also extending the glass transmission window to beyond 20 μm. Lemière *et al*. recently demonstrated a MIR SC in arsenic- and antimony-free chalcogenide glass step-index fiber [75]. Specifically, they obtained 1.7−18 μm SC generation in a 40 mm long and 12 μm core Ge–Se–Te fiber pumped at 8.15 μm with 65 fs pulses delivered by a non-collinear OPA followed by a DFG module [75]. Zhao *et al*. reported a MIR SC spanning from 2 to 16 μm in a 14 cm long low-loss step-index telluride (Ge–Te–AgI) fiber pumped in the normal dispersion regime at 7 μm by 150 fs pulses emitted from an OPA system [56]. Lemière *et al*. also reported SC generation spanning from 2 to 14 μm in a 40 mm long 10 μm core $Ge_{20}Se_{60}Te_{20}/Ge_{20}Se_{70}Te_{10}$ step-index fiber [63]. Significant progress among direct pumping schemes was achieved in 2017 by Hudson *et al*. using as a pump source a holmium-based fiber laser at 2.9 μm [76]. They demonstrated 1.8−9.5 μm MIR SC with an average output power of around 30 mW in a polymer-coated chalcogenide fiber taper with this MIR fiber laser. More recently, a record power of 825 mW was reached using an As_2S_3 fiber-based SC source between 2.5 and 5.0 μm, with Al_2O_3 anti-reflection coatings that were sputtered on chalcogenide fiber tips to increase the launching efficiency up to 82%, making this record output power possible [77].

On the other hand, among the most advanced cascaded fiber-based MIR SC systems, Venck *et al*. in 2020 demonstrated a MIR SC laser source with a bandwidth coverage from 2 to 10 μm in a cascaded silica-ZBLAN-$As_{38}Se_{62}$ fiber system as shown in Fig. 3 [78]. The experimental setup is shown in Fig. 3(a), where a 25 m long ZBLAN fiber was directly pumped with a commercially available 460 ps pulsed fiber laser at 1.55 μm, without any fiber amplifier stage, that generated a SC spectra from 0.7−4.1 μm [see Fig. 3(b)], whose short wavelength edge was then filtered down to 1.9 μm using a germanium anti-reflection coated long-pass filter. The filtered SC was then injected into a 9 m long chalocogenide fiber that generated 2−10 μm SC [see Fig. 3(c)] with an average output power of 16 mW [78]. This technique paves the way for

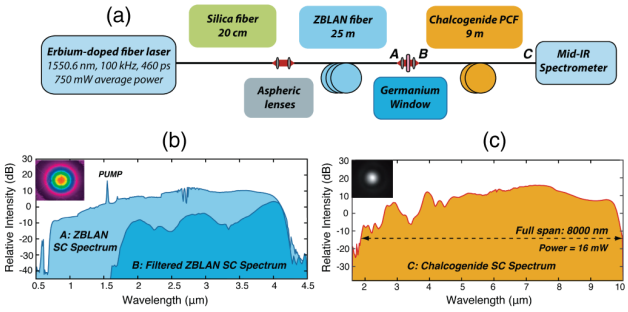

Fig. 3. (a) Experimental setup for mid-infrared SC generation in a cascaded silica-ZBLAN-chalcogenide optical fiber system. (b) Experimental SC spectra at the ZBLAN fiber output (light blue) and after the long-pass germanium filter (dark blue). (c) Experimental SC spectrum at the chalcogenide fiber output (yellow). The insets show the optical mode profiles out of both the (b) ZBLAN and (c) chalcogenide optical fibers. From [78]. Copyright John Wiley and Sons. Reproduced with permission.

low-cost, practical, and robust broadband SC sources without the requirement of MIR pump sources or thulium-doped fiber amplifiers.

A list of the most advanced and recently developed all-fiber-based MIR SC systems is reported in Table 1. In 2021, Woyessa *et al*. demonstrated a stable and portable MIR SC laser source covering the bandwidth from 1.46−10.46 μm with an average output power of 86.6 mW and a repetition rate of 3 MHz in a fiber cascade comprising silica, ZBLAN, and chalcogenide fibers pumped by a 0.5 ns pulsed Er/Yb-master oscillator power amplifier (MOPA) without any amplifier stages [81]. Yan *et al*. demonstrated a watt-level (1.13 W) MIR SC spanning from 2−6.5 μm in a butt coupled ZBLAN and As_2S_3 cascaded fiber system pumped by a 1550 nm pulsed distributed feedback laser and a few stages of a thulium-doped fiber amplifier [82]. In 2019, Petersen *et al*. reported 1.07−7.94 μm MIR SC with an average output power of 41 mW in an all-fiber cascade comprising ZBLAN PCF and $Ge_{10}As_{22}Se_{68}$ PCF taper. A variable repetition rate and 1 ns MOPA pumped ZBLAN PCF generated a SC from 1−4.2 μm, which was then injected into the chalcogenide taper that generated the long-wavelength edge of the SC up to 7.94 μm [83]. In 2018, Martinez *et al*. reported a MIR SC covering the bandwidth from 2 to 11 μm with 139 mW average output power in a cascaded fiber system using concatenated step-index ZBLAN, As_2S_3, and As_2Se_3 fibers. The fiber cascade was pumped at 1.553 μm by a MOPA system and three thulium-doped fiber amplifier stages [84]. In 2014, Kubat *et al*. theoretically reported SC generation spanning from 0.9 to 9 μm with an average output power of 15 mW above 6 μm in a ZBLAN-As_2Se_3 fiber cascade pumped by a thulium laser at 2 μm. The thulium laser pumped ZBLAN step-index fiber generated a SC from 0.9 to 4.1 μm, which is then injected into a 5 μm As_2Se_3 microstructured PCF that generates the long-wavelength edge [72]. Petersen *et al*. demonstrated a MIR cascaded SC generation beyond 7 μm in a silica-fluoride-chalcogenide fiber cascade pumped by a 1.55 μm seed laser and a thulium-doped fiber amplifier [85]. They pumped a commercially available $Ge_{10}As_{22}Se_{68}$-glass PCF with 135 mW of the pump continuum spanning from 3.5−4.4 μm and obtained a SC spectrum up to 7.2 μm with a total output power of 54.5 mW [85]. MIR SC spanning from 1.9−4.8 μm with a record output power of 565 mW was demonstrated by pumping a fiber cascade comprising step-index silica and As_2S_3 fibers with a multistage MOPA system by Gattass *et al*. in 2012 [86]. Commercially available MIR SC sources with an extended bandwidth up to 10 μm and tens of mW output power are now available.

B. Crystalline-Core Fibers

In recent times, a new class of semiconductor fiber with crystalline-core materials has emerged for nonlinear applications [87,88]. These fibers are still clad in silica and retain some of the advantages of conventional glass fibers as they are robust, easy to handle, and can be post-processed using standard techniques. Although fibers with various core materials suitable for MIR SC generation have been fabricated, including Ge, SiGe, ZnSe, and InSb, as of to date, the only semiconductor fibers with dimensions and transmission losses suitable for the observation of SC are those with a Si core [87,88]. Compared to chalcogenide-glass fibers, Si-core fibers offer a high nonlinear refractive index ($1.2 \times 10^{-17} m^2/W$ at wavelengths 2 μm [89,90]) and, due to the high core–cladding index contrast, a tight mode confinement [91], which is useful for both further increasing the nonlinear efficiency and tailoring the dispersion. Coupled with their low losses in the MIR, these properties indicate the potential for Si-core fibers to be used in SC generation in this region. This was confirmed by Ren *et al*. [92]

Table 1. List of Recently Developed Cascaded and All-Fiber Systems for MIR SC Generation

Ref.	Fiber Systems	Amplifiers	SC Bandwidth	Power	Rep. Rate	Pulse Duration
[58]	Silica-ZBLAN fibers	No	0.8−4.5 μm	23 mW	5 kHz	2 ns
[78]	Silica-ZBLAN-As_2Se_3 fibers	No	2−10 μm	16 mW	100 kHz	460 ps
[76]	Chalcogenide taper	No	1.8−9.5 μm	30 mW	42 MHz	230 fs
[79]	Silica-ZBLAN fibers	Yes	1−3.2 μm	1.3 W	5 kHz	2 ns
[80]	Silica-ZBLAN fibers	No	1.8−3.4 μm	5 mW	200 kHz	900 fs
[81]	Doped silica-ZBLAN-chalcogenide fibers	No	1.5−10.5 μm	50 mW	3 MHz	100 ps
[82]	Butt coupled ZBLAN-chalcogenide fibers	Yes	2−6.5 μm	1.13 W	600 kHz	100 ps
[83]	ZBLAN − $Ge_{10}As_{22}Se_{68}$ fiber taper	Yes	1.07−7.94 μm	41 mW	Variable	1 ns
[84]	Silica-ZBLAN-As_2S_3 − As_2Se_3 fibers	Yes	1.6−11 μm	139 mW	800 kHz	1.1 ns
[85]	Silica-ZBLAN-$As_{38}Se_{62}$ fibers	Yes	3.2−7.2 μm	54.3 mW	40 kHz	3 ns
[86]	HNLF-chalcogenide fibers	Yes	1.9−4.8 μm	565 mW	10 MHz	40 ps

when they demonstrated a high brightness and coherent MIR SC from 1.6−5.3 μm in a Si-core fiber that had been asymmetrically tapered to optimize the nonlinear processing in the waist (2.8 μm diameter), while at the same time minimizing the interaction of long-wavelength light with the silica cladding at the output. The fiber was pumped at 3 μm with 100 fs pulses delivered from an OPO system [92].

4. ULTRAVIOLET RANGE

A major challenge in SC generation is to overcome the shortcomings of existing fiber-based SC sources not only in the MIR but also in the UV wavelength range below 400 nm [93,94]. There is a particular need for broadband sources of UV light in applications such as multi-photon fluorescence microscopy for simultaneous coherent excitation of fluorescent proteins [8]. However, UV generation in conventional silica-core fibers is extremely difficult because of many factors such as strong material absorption, the photo-darkening effect, and large normal dispersion. Tapering standard silica PCF has allowed for SC extension below 400 nm, yet limited to 320 nm [93,95].

A. Gas-Filled Hollow-Core Fibers

The use of gas-filled HC fibers for SC generation, especially towards the UV, has seen significant development over the last decade. There are multiple advantages to this approach [96–98]. First, gases can be transparent from the vacuum UV (VUV) up to and across the IR spectral range. The VUV guidance in particular extends far beyond what solid-core fibers can cover. Of course, the actual fiber structure must guide in these regions too. By using anti-resonant "revolver" style fibers, and similar, guidance in the VUV has been demonstrated [99–102]. These guidance windows can extend significantly beyond the transmission region of the glass fiber structure itself, because in anti-resonant regions, the light is almost entirely contained in the hollow core. Second, gases can tolerate much higher intensities than glass, and ionized gas recombines and recovers, so that lasting damage is avoided. Therefore, SC generation at much higher intensity is possible, opening the possibility of ultrafast SC applications that require high energy in a single shot. Third, different gases have nonlinear properties that are different from solid-core fibers and tunable. For example, noble gases do not exhibit Raman scattering, but do have ionization and plasma related nonlinearity, leading to novel soliton dynamics. Alternatively, molecular gases exhibit Raman scattering, but with much narrower linewidths and larger frequency shifts compared to glass. Finally, and perhaps most importantly, the dispersion landscape and nonlinear coefficient can be tuned by simply changing the filling gas pressure or gas mixture. This provides a great degree of freedom for tuning the SC dynamics.

A wide range of nonlinear dynamics has been observed in gas-filled HC fibers, reviewed previously [96–98]. Here we briefly summarize the main SC generation results. Many initial results targeted DW emission in the UV, but can be considered as SC generation by soliton fission [99,100,103–108]; this includes important results on VUV SC generation [99,100], with extension down to 113 nm achieved. The VUV results made use of HC PCF with core diameters around 30 μm, filled with either hydrogen or helium, pumped with ∼30 fs pulses at 800 nm. With much longer pump pulses (500 fs), MI-based SC has also been demonstrated [109] in the visible and IR regions. While these have not yet been extended to the UV, numerical simulations suggest this should be feasible [96]. Recent novelties include utilizing the resonances in ARFs for enhanced SC generation [110], using tapered HC fibers to enhance UV generation [111], and conversion of a Raman frequency comb into a SC that also extends across the deep UV [112].

There are also multiple disadvantages to using gas-filled hollow fibers. The fibers are incompatible with standard fiber technology, they require gas cells and gas and vacuum equipment to operate, they generally require higher power (and hence more expensive) lasers to pump them, and they are not widely available commercially.

B. Novel Glass Fibers

Although these results show great promise, compatibility with the ubiquitous silica platform remains a problem, and there is thus current interest in generating UV light using modified UV-resistant glasses. Significant progress has been made to fabricate low-loss solarization-resistant UV-grade silica PCFs with high OH contents, enabling UV SC generation in the black-light region from 300 to 400 nm and beyond [20]. An alternative solution could be to use ZBLAN-glass optical fibers. For instance, down to the UV (200 nm) to MIR, SC has been generated by pumping into the cladding of a small-core ZBLAN PCF [113].

5. ULTRALOW-NOISE AND COHERENT SC SOURCES

A detrimental feature of typical SC generation, i.e., pumping a fiber in the anomalous dispersion regime, is low temporal coherence and highly stochastic spectral noise [114]. Indeed, for injected pulses with soliton number $N > 16$, noise is stimulated through the nonlinear effects of MI and Raman scattering [2].

A. All-Normal Dispersion Fibers

As an alternative approach, Heidt *et al*. investigated SC generation using high-energy femtosecond pump pulses injected into ANDi PCFs, which exhibit low and flat normal dispersion over the entire bandwidth of the SC bandwidth [27,30,115,116]. In this case, it was shown that only the nonlinear effects of SPM and OWB are responsible for the spectral broadening of the initial pulse [see Fig. 2(b)], which are both known to be highly coherent [117]. Although the concept was introduced already over a decade ago, the strong application-driven demand for low-noise SC sources has resparked scientific interest in ANDi fiber design, as it strongly suppresses the gain for noise-amplifying incoherent nonlinear dynamics [118]. Here, we review the recent progress in the development of ultralow-noise SC sources and their remarkable impact on spectroscopy, imaging, and ultrafast photonics applications.

The superior coherence and noise properties of ANDi SC over conventional SC were experimentally verified, for example,

by measurements of relative intensity noise (RIN), spectral coherence using unequal path Michelson interferometers, dispersive Fourier transformation, and RF beating with stabilized laser diodes [119–123]. However, it is important to note that even the ANDi fiber design does not guarantee the generation of low-noise, coherent SC in every experimental configuration. The competition between coherent and quantum-noise amplifying incoherent nonlinear dynamics typically leads to a threshold pump pulse duration T_{crit} or threshold input soliton number N_{crit} above which the nature of the SC changes from coherent to incoherent. Indeed, as demonstrated in [118], for pump pulse durations longer than ∼1000 fs, the contributions of SRS and FWM are not negligible anymore and start to degrade the SC coherence. Nevertheless, the ANDi fiber design exhibits about 10× higher T_{crit} and 50× higher N_{crit} than its conventional, anomalously pumped counterparts for octave-spanning bandwidths [118]. Another limitation of ANDi SC generation is induced by the coherent coupling of the fiber polarization modes, which can lead to unpredictable fluctuations of the polarization state. This phenomenon is called PMI and is the vectorial aspect of scalar MI. Experimental and numerical studies of PMI effects in ANDi SC generation were reported in weakly birefringent ANDi PCF [124], where the authors demonstrated that decoherence due to PMI starts to appear for pulse durations as short as 120 fs ($N_{crit} \simeq 30$). However, PMI effects can be effectively reduced or suppressed by using highly birefringent polarization-maintaining (PM) ANDi fiber designs [119,120]. Further instabilities related to incoherent polarization mode coupling and Raman amplification of noise were studied in [125–127], with relevance mainly for pump pulse durations in the picosecond regime.

In addition to these limitations induced by different nonlinear effects, the impact of technical noise on ANDi SC generation, such as RIN of the pump pulses at levels higher than the shot-noise limit, was the subject of several recent numerical and experimental studies [128–131], with seemingly contradictory results. While it was demonstrated that a pump laser RIN as low as 0.6% drastically degrades the coherence even for pump pulses as short as 100 fs [128], the RIN of the SC in the central part of the spectrum can actually be lower than the RIN of the pump laser itself [128,129]. This result was unexpected but clearly explained by [130], where the authors determined that the amplitude noise is converted into timing jitter, which affects only the coherence and not the RIN of the SC. However, this timing jitter remains of the order of only 100 attoseconds for practical pump laser parameters, which is up to two orders of magnitude lower than the jitter introduced by conventional soliton-based SC [132,133], and therefore has little practical relevance for most applications. In fact, these studies have revealed the remarkable resilience of ANDi SC generation dynamics to technical pump laser noise under realistic pumping conditions.

Figure 4 shows recent measurements of SC generation in highly birefringent silica ANDi PCF, pumped by 180 fs pulses at 1049 nm [134]. At high pump power, the combined action of SPM and OWB results in a spectrum with superb flatness covering the 670–1390 nm range. The SC exhibits high spectral power density up to 0.4 mW/nm, polarization extinction ratio of 17 dB, RIN as low as 0.54%, and a simple temporal pulse shape with near-linear chirp.

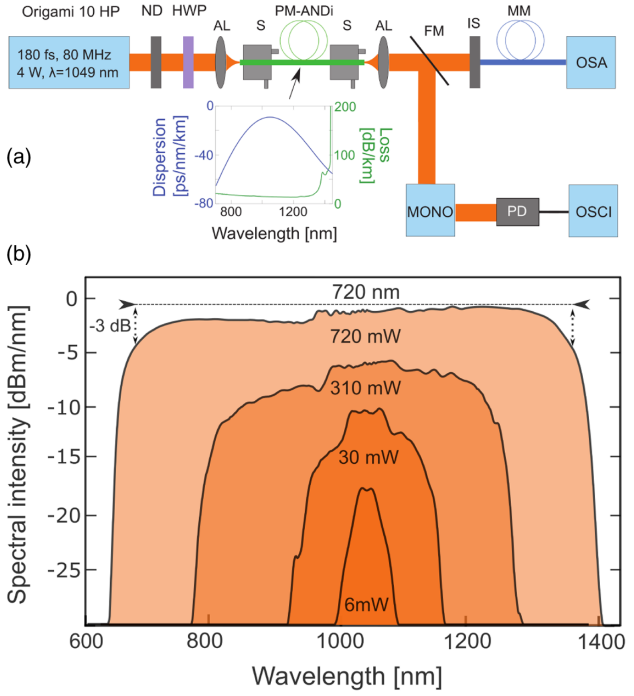

Fig. 4. (a) Experimental setup for ultralow-noise SC generation in a PM-ANDi PCF fiber, including ytterbium femtosecond mode-locked laser (ORIGAMI 10 HP), variable neutral density filter (ND), half-wave plate (HWP), aspheric lenses (AL), 3D translation stages (S), 2 m of PM-ANDi PCF, flip-mirror (FM), integrating sphere (IS), 2 m of multimode pick-up fiber (MM), optical spectrum analyzer (OSA), monochromator (MONO), photodiode (PD), and oscilloscope (OSCI). The inset shows the fiber dispersion and its attenuation spectrum. (b) Experimental SC spectra at the output of the PM-ANDi PCF for average output power of 6 mW to 720 mW with an input beam polarized along the fiber fast axis. Modified with permission from [134]. Copyright 2021 Optica Publishing Group.

Table 2 further summarizes the characteristics of several ANDi SC sources reported in recent literature. For realization of the different fiber designs, a wide range of instruments from the tool box of dispersion engineering in specialty optical fibers has been used, including air-hole microstructures [115,124,129,134–136], microstructures combined with a highly germanium-doped core [137], the integration of different soft glasses into all-solid PCF designs [138], and selective infiltration of PCF holes with liquids [139]. Enabled by the high nonlinearity and transparency of chalcogenide glasses, the spectral coverage of ANDi SC sources has been extended far into the MIR to wavelengths up to 14 μm, e.g., using step-index, tapered or all-solid PCF designs [140–143]. Where available, details of experimental RIN measurements are also listed, such as total bandwidth over which RIN was investigated, measurement method, and spectral filter bandwidth [124,129,134,135,138]. In [124,129], the authors used a setup composed of bandpass filters (10/12 nm), a fast photodiode, and an oscilloscope to measure the spectrally resolved SC RIN. In [124], a high average RIN of 33% was reported, which was attributed to SC coherence degradation by PMI in the weakly birefringent ANDi fiber. In [129], a low average RIN of 1.2% was reported despite the use of a weakly birefringent fiber, owing to a low peak power of the pump pulses. Finally, in [134], the

Table 2. Summary of Coherent SC Generation in ANDi Fibers and Their Noise (RIN) Levels[a]

	SC Properties					Noise Properties			
Ref.	λ_0	P_0	T_0	$\Delta\lambda$	PM	Method	RIN Bandwidth	Filter Bandwidth	RIN
[115]	1050 nm	137 kW	50 fs	905 nm, −20 dB	No			No data	
[115]	790 nm	220 kW	50 fs	880 nm, −20 dB	No			No data	
[124]	1054 nm	44 kW	170 fs	620 nm, −10 dB	No	Osci.	600 nm	10 nm	33 %
[129]	1550 nm	9 kW	120 fs	480 nm, −30 dB	No	Osci.	200 nm	12 nm	1.2 %
[134]	1049 nm	48 kW	180 fs	720 nm, −3 dB	17 dB	Osci.	400 nm	3 nm	0.54 %
[135]	1040 nm	120 kW	230 fs	600 nm, −10 dB	No	ESA	450 nm	100 nm	2 %
[136]	1562 nm	3.3 kW	170 fs	185 nm, −30 dB	No			No data	
[137]	1800 nm	400 kW	70 fs	1500 nm, −20 dB	10 dB			No data	
[138]	1560 nm	22 kW	80 fs	1050 nm, −10 dB	10 dB	ESA	1050 nm	no filter	0.045 %
[139]	1030 nm	62.5 kW	400 fs	500 nm, −60 dB	No			No data	
[140]	5000 nm	160 MW	150 fs	11.2 μm, −30 dB	No			No data	

[a] λ_0, pump wavelength; P_0, peak power; T_0, pulse duration; $\Delta\lambda$, SC bandwidth; PM, polarization maintaining; ESA, electric spectrum analyzer.

authors used highly birefringent, PM ANDi fiber to suppress PMI. They reported a flat spectrally resolved RIN level down to 0.54% over 400 nm using a monochromator with 3 nm filter bandwidth. Based on the summary in Table 2, this was the lowest average RIN value measured using the oscilloscope measurement method. While this is still roughly an order of magnitude larger than the result reported for an ANDi SC used to coherently seed a Tm:fiber amplifier [138], it is important to note that these two RIN measurements cannot be directly compared since the latter was not spectrally resolved but measured over the entire bandwidth of the SC.

B. Selected Application Examples of ANDi SC

For over a decade, commercially available SC sources have made a tremendous impact in advanced spectroscopy and imaging techniques, such as multi-photon microscopy, stimulated emission depletion (STED) microscopy, OCT, and optical resolution photo-acoustic microscopy. Pumped by high-repetition-rate pico- or nanosecond pulsed lasers and equipped with the high beam quality of optical fibers, the brightness of these table-top fiber-based SC sources even surpasses synchrotron beamlines [144]. However, due to the stochastic nature of the nonlinear processes involved in spectral broadening using long pump pulses injected into the anomalous dispersion region of a nonlinear fiber, these SC sources provide spatially but not temporally coherent light and exhibit very large pulse-to-pulse fluctuations of spectral amplitude and phase [2]. The fast-paced advancement of spectroscopic detection and imaging techniques has made this SC noise the predominating factor limiting acquisition speed, sensitivity, or resolution in many applications [145]. The adaptation of low-noise ultrafast ANDi SC sources therefore creates novel opportunities for applications in which the spectral uniformity, temporal profile, or stability of the continuum is of importance and that have hence struggled to incorporate the noise-sensitive and complex conventional SC sources [27].

Hyperspectral SRS microscopy, which is used for label-free, chemical-specific biomedical and mineralogical imaging, is one example of such an application that would benefit from a broadband light source, but the high sensitivity to source noise has so far excluded the use of most nonlinear spectral broadening schemes. As recently demonstrated by Abdolghader *et al*. [146], ANDi SC exhibits very low incremental source noise even when pumped with relatively long 220 fs pulses, and thus represents a viable and easily implementable low-noise source for broadband SRS imaging, greatly enhancing imaging speed in comparison to the alternative of using tunable narrowband lasers. ANDi SC sources were also the key-enabling technology behind the recent demonstration of spectrally resolved scanning near field optical microscopy (SNOM), where commercial SC sources are too noisy to be useful [147]. The new technology enables the investigation of light–matter interaction with spatial resolution on the nanometer scale over a broad spectral bandwidth, relevant in particular to high-speed communications or quantum information processing. The low source noise was also the motivation of implementing ANDi SC in spectral-domain OCT for high axial resolution 3D-imaging, where it led to a paradigm shift, as image quality is no longer limited by the SC noise but by detection shot noise. When compared to state-of-the-art commercial systems, ANDi-SC-based OCT imaging significantly enhances contrast, sensitivity, penetration, and speed, thus paving the way for improved medical diagnosis, e.g., in the early stage detection of skin cancer and other skin diseases [148].

The full power of ANDi SC sources is harnessed by applications that require simultaneously broad spectral bandwidths, short pulses, and high coherence, such as single-beam coherent anti-Stokes Raman scattering (CARS) and other multi-photon microscopy techniques. In contrast to conventional SC, the underlying physics of ANDi SC generation preserve a single ultrafast pulse in the time domain, as shown in Fig. 2, enabling the delivery of fully compressed, broad-bandwidth, few-cycle pulses directly to the focus of highly dispersive microscope objectives. This is most efficiently accomplished by implementing adaptive pulse compression algorithms based on time-domain ptychography on a digital phase shaping device, such as a spatial light modulator, which has led to significant enhancement of signal-to-noise ratios, bandwidth and speed in CARS and multi-photon microscopy compared to alternative techniques [149,150]. In addition, ANDi SC pulses with programmable spectral phase enable coherent control of the nonlinear response of the sample, reducing unwanted

background and amplifying the otherwise weak resonant CARS signal [151]. These advances have led to the development of an extremely versatile platform based on digitally programmable ANDi SC pulses, which combines multiple label-free nonlinear imaging and spectroscopy modalities into a single setup, offering the potential to translate this technology into routine clinical use for disease diagnosis [152]. Even without the relatively expensive digital phase shaping device, broadband multimodal CARS and multi-photon imaging systems based on ANDi SC sources have recently been demonstrated [153].

In ultrafast photonics, the unique temporal properties and high stability of ANDi SC pulses have been exploited for seeding ultra-broadband optical parametric chirped pulse amplification (OPCPA) systems, which have consequently facilitated the generation of coherent soft x-ray radiation and isolated attosecond pulses at high average powers and repetition rates [154,155]. Light pulses with such extreme temporal and spectral properties are enabling new insights into the world of atoms, molecules, and their dynamics, e.g., via photoelectron spectroscopy or XUV microscopy [155]. On the other side of the light spectrum, the seeding of broadband ultrafast thulium- and holmium-doped fiber amplifiers operating at 2 μm wavelength with SC generated in highly birefringent ANDi fibers have resulted in an order of magnitude improvement of amplifier noise over comparable conventionally seeded implementations [138,156]. This wave band is particularly important as a stepping stone for exploration of the molecular fingerprint region in the MIR via nonlinear frequency conversion. Since recent experiments also convincingly demonstrated the advantages of ANDi SC over conventional SC in the construction of stabilized OFCs for frequency metrology [121], these studies have laid the foundations for the next generation of ultralow-noise frequency combs and ultrafast fiber amplifiers operating in the 2 μm spectral region and beyond in the MIR [119].

6. CONCLUSION AND OUTLOOK

The diverse results that have been summarized here clearly show that SC generation in specialty optical fibers is a highly active field of research. We have specifically addressed recent challenges in extending the bandwidth of SC light sources towards both the UV and MIR ranges in areas such as biomedical imaging and molecular spectroscopy. Extensive work over the last 15 years targeting the MIR range has resulted today in compact and reliable cascaded fluoride-chalcogenide fiber systems with watt-level output power over the 2 to 10 μm band. New research directions beyond 10 μm and up to 18 μm are being investigated using telluride-glass fibers [56,75].

While MIR SC fiber technology is becoming more mature, SC generation platforms in the UV and in the deep UV are still developing, and much effort is still needed before compact and reliable UV SC sources can be developed for direct applications. Of particular interest is the 315–400 nm black-light (UV-A) band for applications in chemistry and medicine. UV-grade silica fibers are particularly interesting in this context, as they can generate SC light in this UV-A band by pumping with UV picosecond lasers, but still with low output power and high losses [20]. While SC generation in UV-grade fibers has seen compelling demonstrations, to date the most widely pursued form of UV SC generation is in gas-filled HC fibers, which dispenses with the silica absorption altogether. Such fibers can readily generate high-power broadband UV light down to 100 nm by pumping with femtosecond lasers [99].

Covering further the entire spectral range from the UV to the MIR and beyond into the terahertz requires using scalable high-power few-cycle laser systems combined with DFG in nonlinear quadratic crystals. This has been recently and impressively achieved by Lesko *et al*. [157] and Elu *et al*. [158], who demonstrated record ultra-broadband SC comb generation from 350 nm to 22 μm and from 340 nm to 40 μm, respectively.

We also reviewed the recent advances in ultraflat, low-noise, and coherent SC generation based on ANDi fibers. These results impressively illustrate the potential of ANDi SC sources for applications that so far were not able to use conventional, soliton-based fiber SC sources due to their noise or complex spectra and pulse shapes.

Improved numerical modeling based on the GNLSE has been realized so far, which includes more fiber and pump laser parameters such as all types of noise sources (quantum noise, RIN, time jitter), pulse chirp, complete fiber absorption, and intermodal nonlinear interactions. Furthermore, machine learning analysis of SC generation appears also as a very promising topic towards improvement of SC bandwidth and optimization of both pump laser and fiber parameters [159].

Finally, it is worth stressing here that the diverse numerical and experimental studies of SC generation in specialty fibers over the last 20 years have driven and enabled major parallel advances in developing nonlinear photonic integrated circuits (PICs) based on IR glasses (TiO_2, As_2S_3, Ta_2O_5) and other nonlinear materials (Si, Si_3N_4, SiGe, Ge) [160–164]. Advances in micro-fabrication technology have led to the demonstration of SC generation in a number of PIC platforms, including SC covering the entire MIR first in a chalcogenide chip, and then in a silicon-germanium nanophotonic waveguide. The germanium-based platforms are particularly attractive due to their complementary metal-oxide-semiconductor (CMOS) compatibility, their wide transmission window in the MIR, and their large nonlinearities, enabling SC generation up to 13 μm [165,166].

Funding. H2020 Marie Skłodowska-Curie Actions (SUPUVIR 722380); FP7 Information and Communication Technologies (7326, FP7-7326); Agence Nationale de la Recherche (ANR-15-IDEX-0003, ANR-17-EURE-0002, ANR-20-CE30-0004); Swiss National Science Foundation (PCEFP2_181222); Engineering and Physical Sciences Research Council (EP/P000940/1).

Disclosures. The authors declare no conflicts of interest.

Data Availability. No new data were generated for this review paper.

REFERENCES

1. R. R. Alfano, *The Supercontinuum Laser Source: The Ultimate White Light*, 3rd ed. (Springer, 2016).
2. J. M. Dudley and J. R. Taylor, eds., *Supercontinuum Generation in Optical Fibers* (Cambridge University, 2010).
3. G. Genty, S. Coen, and J. M. Dudley, "Fiber supercontinuum sources," J. Opt. Soc. Am. B **24**, 1771–1785 (2007).
4. T. Udem, R. Holzwarth, and T. W. Hänsch, "Optical frequency metrology," Nature **416**, 233–237 (2002).

5. A. Labruyère, A. Tonello, V. Couderc, G. Huss, and P. Leproux, "Compact supercontinuum sources and their biomedical applications," Opt. Fiber Technol. **18**, 375–378 (2012).
6. LEUKOS, "Scientific supercontinuum lasers," 2021, https://www.leukos-laser.com/.
7. NKT Photonics, "Supercontinuum white light lasers," 2021, https://nktphotonics.com/lasers-fibers/product-category/supercontinuum-lasers.
8. C. Poudel and C. F. Kaminski, "Supercontinuum radiation in fluorescence microscopy and biomedical imaging applications," J. Opt. Soc. Am. B **36**, A139–153 (2019).
9. C. R. Petersen, U. Møller, I. Kubat, B. Zhou, S. Dupont, J. Ramsay, T. Benson, S. Sujecki, N. A. Moneim, Z. Tang, D. Furniss, A. Seddon, and O. Bang, "Mid-infrared supercontinuum covering the 1.4–13.3 μm molecular fingerprint region using ultra-high NA chalcogenide step-index fibre," Nat. Photonics **8**, 830–834 (2014).
10. Y. Wang and S. Dai, "Mid-infrared supercontinuum generation in chalcogenide glass fibers: a brief review," PhotoniX **2**, 9 (2021).
11. G. Hancock, S. J. Horrocks, G. A. D. Ritchie, J. H. van Helden, and R. J. Walker, "Time-resolved detection of the CF_3 photofragment using chirped QCL radiation," J. Phys. Chem. A **112**, 9751–9757 (2008).
12. A. Manninen, T. Kääriäinen, T. Parviainen, S. Buchter, M. Heiliö, and T. Laurila, "Long distance active hyperspectral sensing using high-power near-infrared supercontinuum light source," Opt. Express **22**, 7172–7177 (2014).
13. N. M. Israelsen, C. R. Petersen, A. Barh, D. Jain, M. Jensen, G. Hannesschlöger, P. Tidemand-Lichtenberg, C. Pedersen, A. Podoleanu, and O. Bang, "Real-time high-resolution mid-infrared optical coherence tomography," Light Sci. Appl. **8**, 11 (2019).
14. I. Zorin, R. Su, A. Prylepa, J. Kilgus, M. Brandstetter, and B. Heise, "Mid-infrared Fourier-domain optical coherence tomography with a pyroelectric linear array," Opt. Express **26**, 33428–33439 (2018).
15. Y. Sych, R. Engelbrecht, B. Schmauss, D. Kozlov, T. Seeger, and A. Leipertz, "Broadband time-domain absorption spectroscopy with a ns-pulse supercontinuum source," Opt. Express **18**, 22762–22771 (2010).
16. J. Hult, R. S. Watt, and C. F. Kaminski, "High bandwidth absorption spectroscopy with a dispersed supercontinuum source," Opt. Express **15**, 11385–11395 (2007).
17. C. Amiot, A. Aalto, P. Ryczkowski, J. Toivonen, and G. Genty, "Cavity enhanced absorption spectroscopy in the mid-infrared using a supercontinuum source," Appl. Phys. Lett. **111**, 061103 (2017).
18. J. Troles, S. Venck, S. Cozic, L. Brilland, R. Chahal, M. Meneghetti, J.-L. Adam, C. Boussard-Plédel, B. Bureau, S. Poulain, L. Bodin, F. Joulain, M. Poulain, T. Sylvestre, and G. Huss, "Mid-infrared detection of organic compounds with a 2–10 μm supercontinuum source generated from concatenated fluoride and chalcogenide fibers," Proc. SPIE **11233**, 1123312 (2020).
19. A. Lemière, A. Maldonado, F. Désévédavy, B. Kibler, P. Mathey, G. Gadret, J.-C. Jules, N. P. T. Hoa, T. Suzuki, Y. Ohishi, and F. Smektala, "Towards absorption spectroscopy by means of mid-infrared supercontinuum generation in a step index tellurite fiber," Laser Phys. **31**, 025702 (2021).
20. S. Perret, C. Poudel, A. N. Ghosh, G. Fanjoux, L. Provino, T. Taunay, A. Monteville, D. Landais, C. F. Kaminski, J. M. Dudley, and T. Sylvestre, "Silica-based photonic crystal fiber for the generation of broad band UV radiation," OSA Contin. **3**, 31–42 (2020).
21. D. Jain, R. Sidharthan, P. M. Moselund, S. Yoo, D. Ho, and O. Bang, "Record power, ultra-broadband supercontinuum source based on highly GeO_2 doped silica fiber," Opt. Express **24**, 26667–26677 (2016).
22. G. Agrawal, *Nonlinear Fiber Optics*, 6th ed. (Academic, 2019).
23. P. St.J. Russell, "Photonic crystal fibers," J. Lightwave. Technol. **24**, 4729–4749 (2006).
24. J. K. Ranka, R. S. Windeler, and A. J. Stentz, "Visible continuum generation in air-silica microstructure optical fibers with anomalous dispersion at 800 nm," Opt. Lett. **25**, 25–27 (2000).
25. J. M. Dudley, G. Genty, and S. Coen, "Supercontinuum generation in photonic crystal fiber," Rev. Mod. Phys. **78**, 1135–1184 (2006).
26. A. Mussot, M. Beaugeois, M. Bouazaoui, and T. Sylvestre, "Tailoring strong CW supercontinuum in photonic crystal fibers with two zero dispersion wavelengths," Opt. Express **15**, 11553–11563 (2007).
27. A. M. Heidt, A. Hartung, and H. Bartelt, "Generation of ultrashort and coherent supercontinuum light pulses in all-normal dispersion fibers," in *The Supercontinuum Laser Source: The Ultimate White Light* (Springer, 2016), pp. 247–280.
28. A. M. Heidt, D.-M. Spangenberg, M. Brügmann, E. G. Rohwer, and T. Feurer, "Improved retrieval of complex supercontinuum pulses from XFROG traces using a ptychographic algorithm," Opt. Lett. **41**, 4903–4906 (2016).
29. A. Rampur, D.-M. Spangenberg, G. Stępniewski, D. Dobrakowski, K. Tarnowski, K. Stefańska, A. Paździor, P. Mergo, T. Martynkien, T. Feurer, M. Klimczak, and A. M. Heidt, "Temporal fine structure of all-normal dispersion fiber supercontinuum pulses caused by non-ideal pump pulse shapes," Opt. Express **28**, 16579–16593 (2020).
30. A. M. Heidt, "Pulse preserving flat-top supercontinuum generation in all-normal dispersion photonic crystal fibers," J. Opt. Soc. Am. B **27**, 550–559 (2010).
31. S. Coen, A. H. L. Chau, R. Leonhardt, J. D. Harvey, J. C. Knight, W. J. Wadsworth, and P. St.J. Russell, "White-light supercontinuum generation with 60-ps pump pulses in a photonic crystal fiber," Opt. Lett. **26**, 1356–1358 (2001).
32. J. M. Dudley, L. Provino, N. Grossard, H. Maillotte, R. S. Windeler, B. J. Eggleton, and S. Coen, "Supercontinuum generation in air-silica microstructured fibers with nanosecond and femtosecond pulse pumping," J. Opt. Soc. Am. B **19**, 765–771 (2002).
33. W. J. Wadsworth, N. Joly, J. C. Knight, T. A. Birks, F. Biancalana, and P. St.J. Russell, "Supercontinuum and four-wave mixing with Q-switched pulses in endlessly single-mode photonic crystal fibres," Opt. Express **12**, 299–309 (2004).
34. A. K. Abeeluck, C. Headley, and C. G. Jorgensen, "High-power supercontinuum generation in highly nonlinear, dispersion-shifted fibers by use of a continuous-wave Raman fiber laser," Opt. Lett. **29**, 2163–2165 (2004).
35. T. Sylvestre, A. Vedadi, H. Maillotte, F. Vanholsbeeck, and S. Coen, "Supercontinuum generation using continuous-wave multiwavelength pumping and dispersion management," Opt. Lett. **31**, 2036–2038 (2006).
36. J. C. Travers, A. B. Rulkov, B. A. Cumberland, S. V. Popov, and J. R. Taylor, "Visible supercontinuum generation in photonic crystal fibers with a 400 W continuous wave fiber laser," Opt. Express **16**, 14435–14447 (2008).
37. A. Kudlinski and A. Mussot, "Visible CW-pumped supercontinuum," Opt. Lett. **33**, 2407–2409 (2008).
38. J. M. Dudley, G. Genty, F. Dias, B. Kibler, and N. Akhmediev, "Modulation instability, Akhmediev breathers and continuous wave supercontinuum generation," Opt. Express **17**, 21497–21508 (2009).
39. A. Mussot, T. Sylvestre, L. Provino, and H. Maillotte, "Generation of a broadband single-mode supercontinuum in a conventional dispersion-shifted fiber by use of a subnanosecond microchiplaser," Opt. Lett. **28**, 1820–1822 (2003).
40. C. Lesvigne, V. Couderc, A. Tonello, P. Leproux, A. Barthélémy, S. Lacroix, F. Druon, P. Blandin, M. Hanna, and P. Georges, "Visible supercontinuum generation controlled by intermodal four-wave mixing in microstructured fiber," Opt. Lett. **32**, 2173–2175 (2007).
41. S. Perret, G. Fanjoux, L. Bigot, J. Fatome, G. Millot, J. M. Dudley, and T. Sylvestre, "Supercontinuum generation by intermodal four-wave mixing in a step-index few-mode fibre," APL Photon. **4**, 022905 (2019).
42. P.-A. Champert, V. Couderc, P. Leproux, S. Février, V. Tombelaine, L. Labonté, P. Roy, C. Froehly, and P. Nérin, "White-light supercontinuum generation in normally dispersive optical fiber using original multi-wavelength pumping system," Opt. Express **12**, 4366–4371 (2004).
43. G. Lopez-Galmiche, Z. S. Eznaveh, M. A. Eftekhar, J. A. Lopez, L. G. Wright, F. Wise, D. Christodoulides, and R. A. Correa, "Visible supercontinuum generation in a graded index multimode fiber pumped at 1064 nm," Opt. Lett. **41**, 2553–2556 (2016).

44. K. Krupa, A. Tonello, A. Barthélémy, V. Couderc, B. M. Shalaby, A. Bendahmane, G. Millot, and S. Wabnitz, "Observation of geometric parametric instability induced by the periodic spatial self-imaging of multimode waves," Phys. Rev. Lett. **116**, 183901 (2016).
45. R. Dupiol, A. Bendahmane, K. Krupa, A. Tonello, M. Fabert, B. Kibler, T. Sylvestre, A. Barthelemy, V. Couderc, S. Wabnitz, and G. Millot, "Far-detuned cascaded intermodal four-wave mixing in a multimode fiber," Opt. Lett. **42**, 1293–1296 (2017).
46. M. Chemnitz, M. Gebhardt, C. Gaida, F. Stutzki, J. Kobelke, J. Limpert, A. Tünnermann, and M. A. Schmidt, "Hybrid soliton dynamics in liquid-core fibres," Nat. Commun. **8**, 42 (2017).
47. M. Chemnitz, R. Scheibinger, C. Gaida, M. Gebhardt, F. Stutzki, S. Pumpe, J. Kobelke, A. Tünnermann, J. Limpert, and M. A. Schmidt, "Thermodynamic control of soliton dynamics in liquid-core fibers," Optica **5**, 695–703 (2018).
48. S. Junaid, J. Bierlich, A. Hartung, T. Meyer, M. Chemnitz, and M. A. Schmidt, "Supercontinuum generation in a carbon disulfide core microstructured optical fiber," Opt. Express **29**, 19891–19902 (2021).
49. G. Fanjoux, S. Margueron, J.-C. Beugnot, and T. Sylvestre, "Supercontinuum generation by stimulated Raman-Kerr scattering in a liquid-core optical fiber," J. Opt. Soc. Am. B **34**, 1677–1683 (2017).
50. G. Tao, H. Ebendorff-Heidepriem, A. M. Stolyarov, S. Danto, J. V. Badding, Y. Fink, J. Ballato, and A. F. Abouraddy, "Infrared fibers," Adv. Opt. Photon. **7**, 379–458 (2015).
51. M. Meneghetti, C. Caillaud, R. Chahal, E. Galdo, L. Brilland, J.-L. Adam, and J. Troles, "Purification of Ge–As–Se ternary glasses for the development of high quality microstructured optical fibers," J. Non-Cryst. Solids **503**, 84–88 (2019).
52. C. R. Petersen, R. D. Engelsholm, C. Markos, L. Brilland, C. Caillaud, J. Troles, and O. Bang, "Increased mid-infrared supercontinuum bandwidth and average power by tapering large-mode-area chalcogenide photonic crystal fibers," Opt. Express **25**, 15336–15347 (2017).
53. P. Lucas, Z. Yang, M. K. Fah, T. Luo, S. Jiang, C. Boussard-Pledel, M.-L. Anne, and B. Bureau, "Telluride glasses for far infrared photonic applications," Opt. Mater. Express **3**, 1049–1058 (2013).
54. F. Désévédavy, G. Gadret, J.-C. Jules, B. Kibler, and F. Smektala, "Supercontinuum generation in tellurite optical fibers," in *Technological Advances in Tellurite Glasses*, Springer Ser. Mater. Sci. (Springer, 2017), pp. 254.
55. T. S. Saini, T. H. Tuan, T. Suzuki, and Y. Ohishi, "Coherent mid-IR supercontinuum generation using tapered chalcogenide step-index optical fiber: experiment and modelling," Sci. Rep. **10**, 2236 (2020).
56. Z. Zhao, B. Wu, X. Wang, Z. Pan, Z. Liu, P. Zhang, X. Shen, Q. Nie, S. Dai, and R. Wang, "Mid-infrared supercontinuum covering 2.0–16 μm in a low-loss telluride single-mode fiber," Laser Photon. Rev. **11**, 1700005 (2017).
57. A. N. Ghosh, M. Klimczak, R. Buczynski, J. M. Dudley, and T. Sylvestre, "Supercontinuum generation in heavy-metal oxide glass based suspended-core photonic crystal fibers," J. Opt. Soc. Am. B **35**, 2311–2316 (2018).
58. C. Xia, M. Kumar, O. P. Kulkarni, M. N. Islam, F. L. Terry, M. J. Freeman, M. Poulain, and G. Mazé, "Mid-infrared supercontinuum generation to 4.5 μm in ZBLAN fluoride fibers by nanosecond diode pumping," Opt. Lett. **31**, 2553–2555 (2006).
59. C. Agger, C. Petersen, S. Dupont, H. Steffensen, J. K. Lyngsø, C. L. Thomsen, J. Thøgersen, S. R. Keiding, and O. Bang, "Supercontinuum generation in ZBLAN fibers–detailed comparison between measurement and simulation," J. Opt. Soc. Am. B **29**, 635–645 (2012).
60. M. Michalska, P. Hlubina, and J. Swiderski, "Mid-infrared supercontinuum generation to ∼4.7 μm in a ZBLAN fiber pumped by an optical parametric generator," IEEE Photon. J. **9**, 3200207 (2017).
61. T. Cheng, K. Nagasaka, T. H. Tuan, X. Xue, M. Matsumoto, H. Tezuka, T. Suzuki, and Y. Ohishi, "Mid-infrared supercontinuum generation spanning 2.0 to 15.1 μm in a chalcogenide step-index fiber," Opt. Lett. **41**, 2117–2120 (2016).
62. F. Theberge, N. Berube, S. Poulain, S. Cozic, S. Chatigny, L.-R. Robichaud, L.-P. Pleau, M. Bernier, and R. Vallee, "Infrared supercontinuum generated in concatenated InF_3 and As_2Se_3 fibers," Opt. Express **26**, 13952–13960 (2018).
63. A. Lemière, F. Désévédavy, P. Mathey, P. Froidevaux, G. Gadret, J.-C. Jules, C. Aquilina, B. Kibler, P. Béjot, F. Billard, O. Faucher, and F. Smektala, "Mid-Infrared supercontinuum generation from 2 to 14 μm in arsenic- and antimony-free chalcogenide glass fibers," J. Opt. Soc. Am. B **36**, A183–A192 (2019).
64. V. S. Shiryaev, M. F. Churbanov, G. E. Snopatin, and F. Chenard, "Preparation of low-loss core-clad As-Se glass fibers," Opt. Mater. **48**, 222–225 (2015).
65. K. Sivakumaran and C. K. S. Nair, "Rapid synthesis of chalcogenide glasses of Se-Te-Sb system by microwave irradiation," J. Phys. D **38**, 2476–2479 (2005).
66. D. Thompson, S. Danto, J. D. Musgraves, P. Wachtel, B. Giroire, and K. Richardson, "Microwave assisted synthesis of high purity As_2Se_3 chalcogenide glasses," Eur. J. Glass Sci. Technol. B **54**, 27–34 (2013).
67. Q. Coulombier, L. Brilland, P. Houizot, T. Chartier, T. N. N'Guyen, F. Smektala, G. Renversez, A. Monteville, D. Méchin, T. Pain, H. Orain, J.-C. Sangleboeuf, and J. Trolès, "Casting method for producing low-loss chalcogenide microstructured optical fibers," Opt. Express **18**, 9107–9112 (2010).
68. C. Caillaud, C. Gilles, L. Provino, L. Brilland, T. Jouan, S. Ferre, M. Carras, M. Brun, D. Mechin, J.-L. Adam, and J. Troles, "Highly birefringent chalcogenide optical fiber for polarization-maintaining in the 3–8.5 μm mid-IR window," Opt. Express **24**, 7977–7986 (2016).
69. A. N. Ghosh, M. Meneghetti, C. R. Petersen, O. Bang, L. Brilland, S. Venck, J. Troles, J. M. Dudley, and T. Sylvestre, "Chalcogenide-glass polarization-maintaining photonic crystal fiber for mid-infrared supercontinuum generation," J. Phys. Photon. **1**, 044003 (2019).
70. M. El-Amraoui, G. Gadret, J. C. Jules, J. Fatome, C. Fortier, F. Désévédavy, I. Skripatchev, Y. Messaddeq, J. Troles, L. Brilland, W. Gao, T. Suzuki, Y. Ohishi, and F. Smektala, "Microstructured chalcogenide optical fibers from As_2S_3 glass: towards new IR broadband sources," Opt. Express **18**, 26655–26665 (2010).
71. L. Jiang, X. Wang, F. Guo, B. Wu, Z. Zhao, N. Mi, X. Li, S. Dai, Z. Liu, Q. Nie, and R. Wang, "Fabrication and characterization of chalcogenide polarization-maintaining fibers based on extrusion," Opt. Fiber Technol. **39**, 26–31 (2017).
72. I. Kubat, C. R. Petersen, U. V. Moller, A. Seddon, T. Benson, L. Brilland, D. Mechin, P. M. Moselund, and O. Bang, "Thulium pumped mid-infrared 0.9–9 μm supercontinuum generation in concatenated fluoride and chalcogenide glass fibers," Opt. Express **22**, 3959–3967 (2014).
73. H. Ou, S. Dai, P. Zhang, Z. Liu, X. Wang, F. Chen, H. Xu, B. Luo, Y. Huang, and R. Wang, "Ultrabroad supercontinuum generated from a highly nonlinear Ge-Sb-Se fiber," Opt. Lett. **41**, 3201–3204 (2016).
74. Y. Yu, B. Zhang, X. Gai, C. Zhai, S. Qi, W. Guo, Z. Yang, R. Wang, D.-Y. Choi, S. Madden, and B. Luther-Davies, "1.8–10 μm mid-infrared supercontinuum generated in a step-index chalcogenide fiber using low peak pump power," Opt. Lett. **40**, 1081–1084 (2015).
75. A. Lemière, R. Bizot, F. Désévédavy, G. Gadret, J.-C. Jules, P. Mathey, C. Aquilina, P. Béjot, F. Billard, O. Faucher, B. Kibler, and F. Smektala, "1.7–18 μm mid-infrared supercontinuum generation in a dispersion-engineered step-index chalcogenide fiber," Results Phys. **26**, 104397 (2021).
76. D. D. Hudson, S. Antipov, L. Li, I. Alamgir, T. Hu, M. E. Amraoui, Y. Messaddeq, M. Rochette, S. D. Jackson, and A. Fuerbach, "Toward all-fiber supercontinuum spanning the mid-infrared," Optica **4**, 1163–1166 (2017).
77. L. R. Robichaud, S. Duval, L.-P. Pleau, V. Fortin, S. T. Bah, S. Châtigny, R. Vallée, and M. Bernier, "High-power supercontinuum generation in the mid-infrared pumped by a soliton self-frequency shifted source," Opt. Express **28**, 107–115 (2020).
78. S. Venck, F. St-Hilaire, L. Brilland, A. N. Ghosh, R. Chahal, C. Caillaud, M. Meneghetti, J. Troles, F. Joulain, S. Cozic, S. Poulain, G. Huss, M. Rochette, J. M. Dudley, and T. Sylvestre, "2–10 μm mid-infrared fiber-based supercontinuum laser source: experiment and simulation," Laser Photon. Rev. **14**, 2000011 (2020).

79. C. Xia, M. Kumar, M.-Y. Cheng, R. S. Hegde, M. N. Islam, A. Galvanauskas, H. G. Winful, F. L. Terry, M. J. Freeman, M. Poulain, and G. Mazé, "Power scalable mid-infrared supercontinuum generation in ZBLAN fluoride fibers with up to 1.3 watts time-averaged power," Opt. Express **15**, 865–871 (2007).
80. C. L. Hagen, J. W. Walewski, and S. T. Sanders, "Generation of a continuum extending to the midinfrared by pumping ZBLAN fiber with an ultrafast 1550-nm source," IEEE Photon. Technol. Lett. **18**, 91–93 (2006).
81. G. Woyessa, K. Kwarkye, M. K. Dasa, C. R. Petersen, R. Sidharthan, S. Chen, S. Yoo, and O. Bang, "Power stable 1.5–10.5 μm cascaded mid-infrared supercontinuum laser without thulium amplifier," Opt. Lett. **46**, 1129–1132 (2021).
82. B. Yan, T. Huang, W. Zhang, J. Wang, L. Yang, P. Yang, K. S. Bai, R. Zhao, D. Wu, Y. Liu, X. Li, S. Dai, and Q. Nie, "Generation of watt-level supercontinuum covering 2–6.5 μm in an all-fiber structured infrared nonlinear transmission system," Opt. Express **29**, 4048–4057 (2021).
83. C. R. Petersen, M. B. Lotz, G. Woyessa, A. N. Ghosh, T. Sylvestre, L. Brilland, J. Troles, M. H. Jakobsen, R. Taboryski, and O. Bang, "Nanoimprinting and tapering of chalcogenide photonic crystal fibers for cascaded supercontinuum generation," Opt. Lett. **44**, 5505–5508 (2019).
84. R. A. Martinez, G. Plant, K. Guo, B. Janiszewski, M. J. Freeman, R. L. Maynard, M. N. Islam, F. L. Terry, O. Alvarez, F. Chenard, R. Bedford, R. Gibson, and A. I. Ifarraguerri, "Mid-infrared supercontinuum generation from 1.6 to > 11 μm using concatenated step-index fluoride and chalcogenide fibers," Opt. Lett. **43**, 296–299 (2018).
85. C. R. Petersen, P. M. Moselund, U. Moller, and O. Bang, "Mid-IR supercontinuum generation beyond 7 μm using a silica-fluoride-chalcogenide fiber cascade," Proc. SPIE **9703**, 97030A (2016).
86. R. R. Gattass, L. B. Shaw, V. Q. Nguyen, P. C. Pureza, I. D. Aggarwal, and J. S. Sanghera, "All-fiber chalcogenide-based mid-infrared supercontinuum source," Opt. Fiber Technol. **18**, 345–348 (2012).
87. A. C. Peacock and N. Healy, "Semiconductor optical fibres for infrared applications: a review," Semicond. Sci. Technol. **31**, 103004 (2016).
88. L. Lagonigro, N. Healy, J. R. Sparks, N. F. Baril, P. J. A. Sazio, J. V. Badding, and A. C. Peacock, "Low loss silicon fibers for photonics applications," Appl. Phys. Lett. **96**, 041105 (2010).
89. A. D. Bristow, N. Rotenberg, and H. M. Van Driel, "Two-photon absorption and Kerr coefficients of silicon for 850–2200 nm," Appl. Phys. Lett. **90**, 191104 (2007).
90. H. Ren, L. Shen, D. Wu, O. Aktas, T. Hawkins, J. Ballato, U. J. Gibson, and A. C. Peacock, "Nonlinear optical properties of polycrystalline silicon core fibers from telecom wavelengths into the mid-infrared spectral region," Opt. Mater. Express **9**, 1271–1279 (2019).
91. I. W. Hsieh, X. Chen, X. Liu, J. I. Dadap, N. C. Panoiu, C. Y. Chou, F. Xia, W. M. Green, Y. A. Vlasov, and R. M. Osgood, "Supercontinuum generation in silicon photonic wires," Opt. Express **15**, 15242–15249 (2007).
92. H. Ren, L. Shen, A. F. J. Runge, T. W. Hawkins, J. Ballato, U. Gibson, and A. C. Peacock, "Low-loss silicon core fibre platform for mid-infrared nonlinear photonics," Light Sci. Appl. **8**, 105 (2019).
93. J. C. Travers, "Blue extension of optical fibre supercontinuum generation," J. Opt. **12**, 113001 (2010).
94. T. Sylvestre, A. R. Ragueh, M. W. Lee, B. Stiller, G. Fanjoux, B. Barviau, A. Mussot, and A. Kudlinski, "Black-light continuum generation in a silica-core photonic crystal fiber," Opt. Lett. **37**, 130–132 (2012).
95. A. Kudlinski, A. K. George, J. C. Knight, J. C. Travers, A. B. Rulkov, S. V. Popov, and J. R. Taylor, "Zero-dispersion wavelength decreasing photonic crystal fibers for ultraviolet-extended supercontinuum generation," Opt. Express **14**, 5715–5722 (2006).
96. J. C. Travers, W. Chang, J. Nold, N. Y. Joly, and P. St.J. Russell, "Ultrafast nonlinear optics in gas-filled hollow-core photonic crystal fibers [invited]," J. Opt. Soc. Am. B **28**, A11–26 (2011).
97. P. St.J. Russell, P. Hölzer, W. Chang, A. Abdolvand, and J. C. Travers, "Hollow-core photonic crystal fibres for gas-based nonlinear optics," Nat. Photonics **8**, 278–286 (2014).
98. C. Markos, J. C. Travers, A. Abdolvand, B. J. Eggleton, and O. Bang, "Hybrid photonic-crystal fiber," Rev. Mod. Phys. **89**, 045003 (2017).
99. F. Belli, A. Abdolvand, W. Chang, J. C. Travers, and P. St.J. Russell, "Vacuum ultraviolet to infrared supercontinuum in hydrogen-filled photonic crystal fiber," Optica **2**, 292–300 (2015).
100. A. Ermolov, K. F. Mak, M. H. Frosz, J. C. Travers, and P. St.J. Russell, "Supercontinuum generation in the vacuum ultraviolet through dispersive-wave and soliton-plasma interaction in a noble-gas-filled hollow-core photonic crystal fiber," Phys. Rev. A **92**, 033821 (2015).
101. B. Winter, D. Vorobiev, B. Fleming, E. Witt, W. Gilliam, K. R. Rusimova, S. Yerolatsitis, T. A. Birks, and W. J. Wadsworth, "185nm guidance in a hollow core optical fibre," in *Frontiers in Optics + Laser Science APS/DLS* (Optical Society of America, 2019), paper JTu3A.19.
102. D. E. Couch, D. D. Hickstein, D. D. Hickstein, D. G. Winters, S. J. Backus, S. J. Backus, M. S. Kirchner, S. R. Domingue, J. J. Ramirez, C. G. Durfee, M. M. Murnane, and H. C. Kapteyn, "Ultrafast 1 MHz vacuum-ultraviolet source via highly cascaded harmonic generation in negative-curvature hollow-core fibers," Optica **7**, 832–837 (2020).
103. N. Y. Joly, J. Nold, W. Chang, P. Hölzer, A. Nazarkin, G. K. L. Wong, F. Biancalana, and P. St.J. Russell, "Bright spatially coherent wavelength-tunable deep-UV Laser source using an Ar-filled photonic crystal fiber," Phys. Rev. Lett. **106**, 203901 (2011).
104. K. F. Mak, J. C. Travers, P. Hölzer, N. Y. Joly, and P. St.J. Russell, "Tunable vacuum-UV to visible ultrafast pulse source based on gas-filled Kagome-PCF," Opt. Express **21**, 10942–10953 (2013).
105. M. Cassataro, D. Novoa, M. C. Günendi, N. N. Edavalath, M. H. Frosz, J. C. Travers, and P. St.J. Russell, "Generation of broadband mid-IR and UV light in gas-filled single-ring hollow-core PCF," Opt. Express **25**, 7637–7644 (2017).
106. F. Yu, M. Cann, A. Brunton, W. Wadsworth, and J. Knight, "Single-mode solarization-free hollow-core fiber for ultraviolet pulse delivery," Opt. Express **26**, 10879–10887 (2018).
107. A. I. Adamu, M. S. Habib, C. R. Petersen, J. E. A. Lopez, B. Zhou, A. Schölzgen, M. Bache, R. Amezcua-Correa, O. Bang, and C. Markos, "Deep-UV to mid-IR supercontinuum generation driven by Mid-IR ultrashort pulses in a gas-filled hollow-core fiber," Sci. Rep. **9**, 4446 (2019).
108. A. I. Adamu, M. S. Habib, C. R. Smith, J. E. A. Lopez, P. U. Jepsen, R. Amezcua-Correa, O. Bang, and C. Markos, "Noise and spectral stability of deep-UV gas-filled fiber-based supercontinuum sources driven by ultrafast mid-IR pulses," Sci. Rep. **10**, 4912 (2020).
109. F. Tani, J. C. Travers, and P. St.J. Russell, "PHz-wide Supercontinua of nondispersing subcycle pulses generated by extreme modulational instability," Phys. Rev. Lett. **111**, 033902 (2013).
110. R. Sollapur, D. Kartashov, M. Zürch, A. Hoffmann, T. Grigorova, G. Sauer, A. Hartung, A. Schwuchow, J. Bierlich, J. Kobelke, M. Chemnitz, M. A. Schmidt, and C. Spielmann, "Resonance-enhanced multi-octave supercontinuum generation in antiresonant hollow-core fibers," Light Sci. Appl. **6**, e17124 (2017).
111. M. I. Suresh, J. Hammer, N. Y. Joly, P. St.J. Russell, and F. Tani, "Deep-UV-enhanced supercontinuum generated in tapered gas-filled photonic crystal fiber," arXiv:2107.05417 [physics] (2021).
112. S.-F. Gao, Y.-Y. Wang, F. Belli, C. Brahms, P. Wang, and J. C. Travers, "From Raman frequency combs to supercontinuum generation in nitrogen-filled hollow-core anti-resonant fiber," arXiv:2011.01656 [physics] (2020).
113. X. Jiang, N. Y. Joly, M. A. Finger, F. Babic, G. K. L. Wong, J. C. Travers, and P. St.J. Russell, "Deep-ultraviolet to mid-infrared supercontinuum generated in solid-core ZBLAN photonic crystal fiber," Nat. Photonics **9**, 133–139 (2015).
114. B. Wetzel, A. Stefani, L. Larger, P. A. Lacourt, J. M. Merolla, T. Sylvestre, A. Kudlinski, A. Mussot, G. Genty, F. Dias, and J. M. Dudley, "Real-time full bandwidth measurement of spectral noise in supercontinuum generation," Sci. Rep. **2**, 882 (2012).
115. A. M. Heidt, A. Hartung, G. W. Bosman, P. Krok, E. G. Rohwer, H. Schwoerer, and H. Bartelt, "Coherent octave spanning near-infrared

and visible supercontinuum generation in all-normal dispersion photonic crystal fibers," Opt. Express **19**, 3775–3787 (2011).
116. A. Hartung, A. M. Heidt, and H. Bartelt, "Design of all-normal dispersion microstructured optical fibers for pulse-preserving supercontinuum generation," Opt. Express **19**, 7742–7749 (2011).
117. C. Finot, B. Kibler, L. Provost, and S. Wabnitz, "Beneficial impact of wave-breaking for coherent continuum formation in normally dispersive nonlinear fibers," J. Opt. Soc. Am. B **25**, 1938–1948 (2008).
118. A. M. Heidt, J. S. Feehan, J. H. V. Price, and T. Feurer, "Limits of coherent supercontinuum generation in normal dispersion fibers," J. Opt. Soc. Am. B **34**, 764–775 (2017).
119. A. Rampur, D.-M. Spangenberg, B. Sierro, P. Hänzi, M. Klimczak, and A. M. Heidt, "Perspective on the next generation of ultra-low noise fiber supercontinuum sources and their emerging applications in spectroscopy, imaging, and ultrafast photonics," Appl. Phys. Lett. **118**, 240504 (2021).
120. Y. Liu, Y. Zhao, J. Lyngsø, S. You, W. L. Wilson, H. Tu, and S. A. Boppart, "Suppressing short-term polarization noise and related spectral decoherence in all-normal dispersion fiber supercontinuum generation," J. Lightwave Technol. **33**, 1814–1820 (2015).
121. N. Nishizawa, T. Niinomi, Y. Nomura, L. Jin, and Y. Ozeki, "Octave spanning coherent supercontinuum comb generation based on Er-doped fiber lasers and their characterization," IEEE J. Sel. Top. Quantum Electron. **24**, 5100409 (2018).
122. M. Klimczak, G. Sobon, R. Kasztelanic, K. M. Abramski, and R. Buczynski, "Direct comparison of shot-to-shot noise performance of all normal dispersion and anomalous dispersion supercontinuum pumped with sub-picosecond pulse fiber-based laser," Sci. Rep. **6**, 19284 (2016).
123. K. Tarnowski, T. Martynkien, P. Mergo, J. Sotor, and G. Sobon, "Compact all-fiber source of coherent linearly polarized octave-spanning supercontinuum based on normal dispersion silica fiber," Sci. Rep. **9**, 12313 (2019).
124. I. B. Gonzalo, R. D. Engelsholm, M. P. Sørensen, and O. Bang, "Polarization noise places severe constraints on coherence of all-normal dispersion femtosecond supercontinuum generation," Sci. Rep. **8**, 6579 (2018).
125. I. B. Gonzalo and O. Bang, "Role of the Raman gain in the noise dynamics of all-normal dispersion silica fiber supercontinuum generation," J. Opt. Soc. Am. B **35**, 2102–2110 (2018).
126. J. S. Feehan, E. Brunetti, S. Yoffe, W. Li, S. M. Wiggins, D. A. Jaroszynski, and J. H. V. Price, "Noise-related polarization dynamics for femto and picosecond pulses in normal dispersion fibers," Opt. Express **28**, 21447–21463 (2020).
127. J. S. Feehan and J. H. V. Price, "Decoherence due to XPM-assisted Raman amplification for polarization or wavelength offset pulses in all-normal dispersion supercontinuum generation," J. Opt. Soc. Am. B **37**, 635–644 (2020).
128. E. Genier, P. Bowen, T. Sylvestre, J. M. Dudley, P. Moselund, and O. Bang, "Amplitude noise and coherence degradation of femtosecond supercontinuum generation in all-normal-dispersion fibers," J. Opt. Soc. Am. B **36**, A161–A167 (2019).
129. D. S. S. Rao, R. D. Engelsholm, I. B. Gonzalo, B. Zhou, P. Bowen, P. M. Moselund, O. Bang, and M. Bache, "Ultra-low-noise supercontinuum generation with a flat near-zero normal dispersion fiber," Opt. Lett. **44**, 2216–2219 (2019).
130. B. Sierro and A. M. Heidt, "Noise amplification in all-normal dispersion fiber supercontinuum generation and its impact on ultrafast photonics applications," OSA Contin. **3**, 2347–2361 (2020).
131. Z. Eslami, P. Ryczkowski, L. Salmela, and G. Genty, "Low-noise octave-spanning mid-infrared supercontinuum generation in a multimode chalcogenide fiber," Opt. Lett. **45**, 3103–3106 (2020).
132. J. Rothhardt, A. M. Heidt, S. Hädrich, S. Demmler, J. Limpert, and A. Tünnermann, "High stability soliton frequency-shifting mechanisms for laser synchronization applications," J. Opt. Soc. Am. B **29**, 1257–1262 (2012).
133. Y. Hua, G. Zhou, W. Liu, M. Xin, F. X. Kärtner, and G. Chang, "Femtosecond two-color source synchronized at 100-as-precision based on SPM-enabled spectral selection," Opt. Lett. **45**, 3410–3413 (2020).
134. E. Genier, S. Grelet, R. D. Engelsholm, P. Bowen, P. M. Moselund, O. Bang, J. M. Dudley, and T. Sylvestre, "Ultra-flat, low-noise, and linearly polarized fiber supercontinuum source covering 670–1390 nm," Opt. Lett. **46**, 1820–1823 (2021).
135. B. Resan, S. Kurmulis, V. Markovic, and K. J. Weingarten, "1% RMS amplitude noise from a 30 fs continuum based source tunable from 800 to 1250 nm," Opt. Express **24**, 14960–14965 (2016).
136. K. Chow, Y. Takushima, C. Lin, C. Shu, and A. Bjarklev, "Flat supercontinuum generation based on normal dispersion nonlinear photonic crystal fibre," Electron. Lett. **42**, 989–991 (2006).
137. K. Tarnowski, T. Martynkien, P. Mergo, K. Poturaj, A. Anuszkiewicz, P. Béjot, F. Billard, O. Faucher, B. Kibler, and W. Urbanczyk, "Polarized all-normal dispersion supercontinuum reaching 2.5 mm generated in a birefringent microstructured silica fiber," Opt. Express **25**, 27452–27463 (2017).
138. A. Rampur, Y. Stepanenko, G. Stępniewski, T. Kardaś, D. Dobrakowski, D.-M. Spangenberg, T. Feurer, A. Heidt, and M. Klimczak, "Ultra low-noise coherent supercontinuum amplification and compression below 100 fs in an all-fiber polarization-maintaining thulium fiber amplifier," Opt. Express **27**, 35041–35051 (2019).
139. H. V. Le, V. T. Hoang, H. T. Nguyen, V. C. Long, R. Buczynski, and R. Kasztelanic, "Supercontinuum generation in photonic crystal fibers infiltrated with tetrachloroethylene," Opt. Quantum Electron. **53**, 187 (2021).
140. Y. Yuan, P. Yang, X. Peng, Z. Cao, S. Ding, N. Zhang, Z. Liu, P. Zhang, X. Wang, and S. Dai, "Ultrabroadband and coherent mid-infrared supercontinuum generation in all-normal dispersion Te-based chalcogenide all-solid microstructured fiber," J. Opt. Soc. Am. B **37**, 227–232 (2020).
141. N. Zhang, X. Peng, Y. Wang, S. Dai, Y. Yuan, J. Su, G. Li, P. Zhang, P. Yang, and X. Wang, "Ultrabroadband and coherent mid-infrared supercontinuum generation in Te-based chalcogenide tapered fiber with all-normal dispersion," Opt. Express **27**, 10311–10319 (2019).
142. K. Jiao, J. Yao, Z. Zhao, X. Wang, N. Si, X. Wang, P. Chen, Z. Xue, Y. Tian, B. Zhang, P. Zhang, S. Dai, Q. Nie, and R. Wang, "Mid-infrared flattened supercontinuum generation in all-normal dispersion tellurium chalcogenide fiber," Opt. Express **27**, 2036–2043 (2019).
143. K. Nagasaka, L. Liu, T. H. Tuan, T. Cheng, M. Matsumoto, H. Tezuka, T. Suzuki, and Y. Ohishi, "Supercontinuum generation in chalcogenide double-clad fiber with near zero-flattened normal dispersion profile," J. Opt. **19**, 095502 (2017).
144. C. R. Petersen, P. M. Moselund, L. Huot, L. Hooper, and O. Bang, "Towards a table-top synchrotron based on supercontinuum generation," Infrared Phys. Technol. **91**, 182–186 (2018).
145. M. Jensen, I. B. Gonzalo, R. D. Engelsholm, M. Maria, N. M. Israelsen, A. Podoleanu, and O. Bang, "Noise of supercontinuum sources in spectral domain optical coherence tomography," J. Opt. Soc. Am. B **36**, A154–A160 (2019).
146. P. Abdolghader, A. F. Pegoraro, N. Y. Joly, A. Ridsdale, R. Lausten, F. Légaré, and A. Stolow, "All normal dispersion nonlinear fibre supercontinuum source characterization and application in hyperspectral stimulated Raman scattering microscopy," Opt. Express **28**, 35997–36008 (2020).
147. K. J. Kaltenecker, D. S. S. Rao, M. Rasmussen, H. B. Lassen, E. J. R. Kelleher, E. Krauss, B. Hecht, N. A. Mortensen, L. Gruener-Nielsen, C. Markos, O. Bang, N. Stenger, and P. U. Jepsen, "Near-infrared nanospectroscopy using a low-noise supercontinuum source," APL Photon. **6**, 066106 (2021).
148. D. S. S. Rao, M. Jensen, L. Grüner-Nielsen, J. T. Olsen, P. Heiduschka, B. Kemper, J. Schnekenburger, M. Glud, M. Mogensen, N. M. Israelsen, and O. Bang, "Shot-noise limited, supercontinuum based optical coherence tomography," Light Sci. Appl. **10**, 133 (2021).
149. R. Viljoen, P. Neethling, D. Spangenberg, A. Heidt, H.-M. Frey, T. Feurer, and E. Rohwer, "Implementation of temporal ptychography algorithm, i2PIE, for improved single-beam coherent anti-Stokes Raman scattering measurements," J. Opt. Soc. Am. B **37**, A259–A265 (2020).

150. G. Dwapanyin, D. Spangenberg, A. Heidt, T. Feurer, G. Bosman, P. Neethling, and E. Rohwer, "Generalized spectral phase-only time-domain ptychographic phase reconstruction applied in nonlinear microscopy," J. Opt. Soc. Am. B **37**, A285–A292 (2020).
151. H. Tu and S. A. Boppart, "Coherent anti-Stokes Raman scattering microscopy: overcoming technical barriers for clinical translation," J. Biophoton. **7**, 9–22 (2014).
152. H. Tu, Y. Liu, D. Turchinovich, M. Marjanovic, J. K. Lyngsø, J. Lægsgaard, E. J. Chaney, Y. Zhao, S. You, W. L. Wilson, B. Xu, M. Dantus, and S. A. Boppart, "Stain-free histopathology by programmable supercontinuum pulses," Nat. Photonics **10**, 534–540 (2016).
153. K. P. Herdzik, K. N. Bourdakos, P. B. Johnson, A. P. Lister, A. P. Pitera, C.-Y. Guo, P. Horak, D. J. Richardson, J. H. Price, and S. Mahajan, "Multimodal spectral focusing CARS and SFG microscopy with a tailored coherent continuum from a microstructured fiber," Appl. Phys. B **126**, 84 (2020).
154. M. Krebs, S. Hädrich, S. Demmler, J. Rothhardt, A. Zar, L. Chipperfield, J. Limpert, and A. Tünnermann, "Towards isolated attosecond pulses at megahertz repetition rates," Nat. Photonics **7**, 555–559 (2013).
155. J. Rothhardt, S. Hädrich, J. Delagnes, E. Cormier, and J. Limpert, "High average power near-infrared few-cycle lasers," Laser Photon. Rev. **11**, 1700043 (2017).
156. A. M. Heidt, J. M. Hodasi, A. Rampur, D.-M. Spangenberg, M. Ryser, M. Klimczak, and T. Feurer, "Low noise all-fiber amplification of a coherent supercontinuum at 2 μm and its limits imposed by polarization noise," Sci. Rep. **10**, 16734 (2020).
157. D. M. B. Lesko, H. Timmers, S. Xing, A. Kowligy, A. J. Lind, and S. A. Diddams, "A six-octave optical frequency comb from a scalable few-cycle erbium fibre laser," Nat. Photonics **15**, 281–286 (2021).
158. U. Elu, L. Maidment, L. Vamos, F. Tani, D. Novoa, M. H. Frosz, V. Badikov, D. Badikov, V. Petrov, P. St.J. Russell, and J. Biegert, "Seven-octave high-brightness and carrier-envelope-phase-stable light source," Nat. Photonics **15**, 277–280 (2021).
159. L. Salmela, C. Lapre, J. M. Dudley, and G. Genty, "Machine learning analysis of rogue solitons in supercontinuum generation," Sci. Rep. **10**, 9596 (2020).
160. M. R. E. Lamont, B. Luther-Davies, D.-Y. Choi, S. Madden, and B. J. Eggleton, "Supercontinuum generation in dispersion engineered highly nonlinear As_2S_3 chalcogenide planar waveguide," Opt. Express **16**, 14938–14944 (2008).
161. R. K. W. Lau, M. R. E. Lamont, A. G. Griffith, Y. Okawachi, M. Lipson, and A. L. Gaeta, "Octave-spanning mid-infrared supercontinuum generation in silicon nanowaveguides," Opt. Lett. **39**, 4518–4521 (2014).
162. Y. Yu, X. Gai, P. Ma, D.-Y. Choi, Z. Yang, R. Wang, S. Debbarma, S. J. Madden, and B. Luther-Davies, "A broadband, quasi-continuous, mid-infrared supercontinuum generated in a chalcogenide glass waveguide," Laser Photon. Rev. **8**, 792–798 (2014).
163. D. Grassani, E. Tagkoudi, H. Guo, C. Herkommer, F. Yang, T. J. Kippenberg, and C.-S. Brès, "Mid infrared gas spectroscopy using efficient fiber laser driven photonic chip-based supercontinuum," Nat. Commun. **10**, 1553 (2019).
164. N. Singh, D. D. Hudson, Y. Yu, C. Grillet, S. D. Jackson, A. Casas-Bedoya, A. Read, P. Atanackovic, S. G. Duvall, S. Palomba, B. Luther-Davies, S. Madden, D. J. Moss, and B. J. Eggleton, "Midinfrared supercontinuum generation from 2 to 6 μm in a silicon nanowire," Optica **2**, 797–802 (2015).
165. M. Sinobad, C. Monat, B. Luther-Davies, P. Ma, S. Madden, D. J. Moss, A. Mitchell, D. Allioux, R. Orobtchouk, S. Boutami, J.-M. Hartmann, J.-M. Fedeli, and C. Grillet, "Mid-infrared octave spanning supercontinuum generation to 8.5 μm in silicon-germanium waveguides," Optica **5**, 360–366 (2018).
166. M. Montesinos-Ballester, C. Lafforgue, J. Frigerio, A. Ballabio, V. Vakarin, Q. Liu, J. M. Ramirez, X. Le Roux, D. Bouville, A. Barzaghi, C. Alonso-Ramos, L. Vivien, G. Isella, and D. Marris-Morini, "On-chip mid-infrared supercontinuum generation from 3 to 13 μm wavelength," ACS Photon. **7**, 3423–3429 (2020).